Deformation, seismicity, and fluids: Results of the 2004/2005 water injection experiment at the KTB/Germany

T. Jahr,[1] G. Jentzsch,[1] A. Gebauer,[1] and T. Lau[2]

[1]   During the past decades, the research into fluid-controlled geodynamic processes in the upper crust of the Earth is put foreward regarding the stress accumulation, deformation, and seismicity. In a large-scale injection experiment at the deep borehole site KTB (Kontinentale Tiefbohrung der Bundesrepublik Deutschland) in Germany, more than 84.000 m^3 fresh water was injected in 4000 m depth over 10 months, and a lot of geoscientific investigations were connected to this injection test. The pore-pressure change of more than 10 MPa yielded an induced deformation, which was detected by a tiltmeter array. The used five borehole tiltmeters of the ASKANIA type with a resolution of better than 1 nrad belong to the most sensitive tiltmeters worldwide. The poro-elastic finite-element modeling used for the interpretation of the observed tilts revealed an uplift of 3.1 mm above the injection point. Furthermore, it was shown that the induced stress and deformation fields depend mainly on the fluids inside the fault zones, particularly the SE2-reflector which is the Franconian fault zone, and the local Nottersdorf fault: While the maximum pore pressure is concentrated close to the injection point at the SE2 zone, the maximum deformation of about 3 cm is located at the intersection line of both faults in 4 km depth. The area of the modeled maximum deformation is highly correlated with the region of the observed induced seismicity, thus linking seismicity and deformation. The connection of tilt observation and modeling provides a useful tool for the investigation of fluid coupled geoprocesses.

1. Introduction

[2]   In 1997, the Journal of Geophysical Research, No. 102, published a special section containing 20 papers about the German super-deep drilling project KTB, covering all aspects of the German Continental Deep Drilling Program like geology, crustal and tectonic evolution, fluids, crustal seismic reflections, 3D-interpretation of potential field data, borehole logging, etc. [see, e.g., *Haak and Jones*, 1997; *Emmermann and Lauterjung*, 1997]. The geological and geophysical boundary conditions were summarized, e.g., by *Harjes et al.* [1997]. A first injection experiment in the kilometre scale was carried out in 1994 in the 9101 m deep main borehole, during which considerable seismicity was induced [*Zoback and Harjes*, 1997; *Baisch and Harjes*, 2003]. The evaluation of the data revealed that fluid migration plays a major role in relation to stress accumulation, deformation and seismicity in the upper crust of the Earth. Basically, this is an old relation becoming more and more prominent in the last years in earthquake and volcanic research, regarding strong single as well as swarm earth-

quake events due to fluid flow in fractured rocks [*Battaglia et al.*, 1999; *Miller et al.*, 2004; *Bräuer et al.*, 2005; *Hill and Prejean*, 2005; *Reches and Ito*, 2007]. However, the interaction of the geodynamic parameters of the upper crust and the fluids is still poorly known. Early experiments in the year 1976 [*Raleigh et al.*, 1976] mark a starting point for such geodynamic investigations. At the super deep borehole KTB in Germany with well-known input parameters and a variety of experiments a significant improvement of such geodynamic investigations could be achieved [*Harms et al.*, 2007; *Kümpel et al.*, 2006]. A similar experiment was conducted in Japan, but at a much lower depth [*Fujimori et al.*, 2001]. On the other hand, in engineering geophysics tilt measurements are meanwhile standard to monitor, e.g., land slides or the exploitation of shallow reservoirs [e.g., *Tofani and Horath*, 1990].

[3]   The experiments at KTB address this special extension of fluid flow and fluid systems in Earth's crystalline crust. These processes have a great impact on rheology, as well as the dynamics and mechanical stability of the crust. The KTB boreholes offer a unique chance to study these parameters under in situ conditions, which is of fundamental geoscientific interest, especially in those areas in which fluid and thermal reservoirs are situated. Further, such experiments are also important for the society related to the understanding of safe disposal of critical wastes. Seismogenesis, particularly in connection with large lake reser-

[1]Applied Geophysics, Institute of Geosciences, Friedrich-Schiller-University Jena, Jena, Germany.
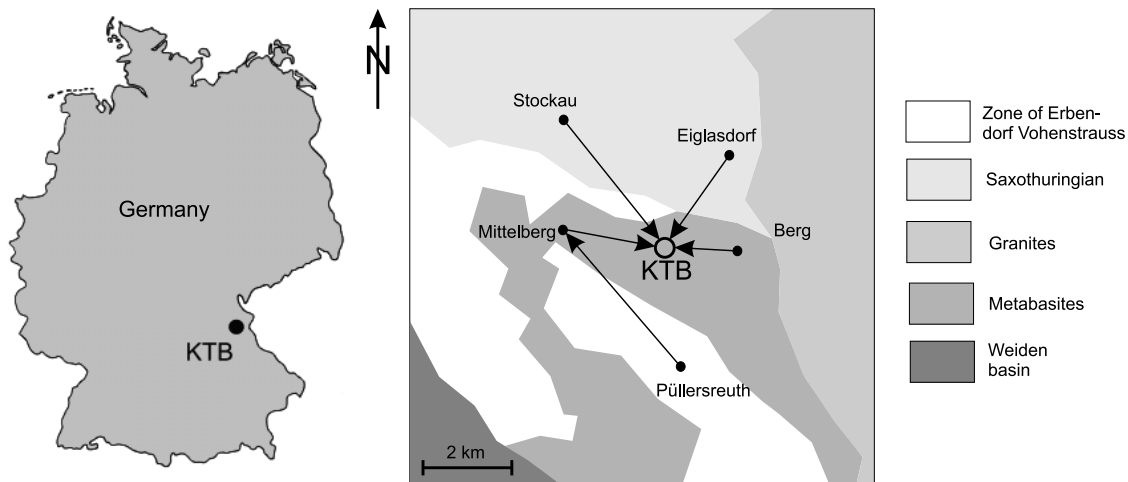[2]Max-Planck-Institute of Meteorology, Hamburg, Germany.

Figure 1. Investigation area around the KTB location in Upper Palatinate in Germany: Main geological complexes are given. The KTB tiltmeter array with five stations (solid circle) and the wireless local area network (WLAN) data connection to the KTB site are shown, marked by the arrows.

voirs, is another main issue. These fluid flow processes in the crystalline crust cause deformation which can be monitored by tilt measurements. Numerical modeling constrained by observed tilt provides insight into such processes.

2. Two KTB Hydraulic Experiments From 2002 to 2004

[4] A production test was conducted from June 2002 to June 2003, using the open hole section of the KTB pilot hole at 3850 to 4000 m depth [*Kümpel et al.*, 2006]. An initial production rate of 29 l/min yielded a fluid-level draw down of only 280 m after four months, less than one-third of the expected value. Therefore the production rate was increased up to 58 l/min with a maximum draw down of 605 m at the end of the pump experiment in June 2003. Various geophysical, hydraulic, and geochemical parameters were monitored online at the site, however, the tiltmeter array started operating not earlier than in November 2003. Tilt effects, induced by pumping, could therefore only be observed for the one-year recovery phase from the production test. It can be expected, that the backflow affected also the pore pressure and the associated deformation of the upper crust. Therefore, it may rest assured that this deformation superimposed the run-in period of the tiltmeters and their installations.

[5] The injection experiment was conducted over ten months from June 2004 until April 2005 [*Kümpel et al.*, 2006]. Fresh water was injected into the pilot bore hole with a rate of about 180 l/min and with a total volume of 84,600 m^3. Well-head pressure gradually dropped from about 120 bar to 90 bar within the first two months, then it slowly increased to 115 bar in April 2005. Again several parallel running research projects dealt with the monitoring of seismicity, geoelectric parameter changes, fluid flow, hydraulics, geochemistry of gases, rheology, rock properties, and pressure studies, all associated with numerical modeling [*Gräsle et al.*, 2006; *Lippmann et al.*, 2005; *Stober and Bucher*, 2005; *Möller et al.*, 2005]. About 3000 micro-seismic events were detected by the borehole

geophone in the KTB-HB (main borehole), and 150 events by the local seismic network at the surface. The analysis of the seismic events showed, that the induced seismicity was controlled by the fluid migrating into the crustal fault system. It is triggered by pore pressure perturbations as low as $0.01-1.00$ bar at the hypocenters [*Shapiro et al.*, 2006]. Most important was the fact that seismicity started after the injected water volume was approximately equivalent to the amount previously extracted by the pump experiment. Thus it could be expected, that an observable deformation of the upper crust was first detectable not earlier than some months after the start of the injection in June 2004.

[6] Our approach to observe the injection-induced deformation of the Earth's upper crust by using high-resolution tiltmeters in boreholes near the surface was aimed at the studying of the interaction of fluid migration, pore-pressure variation and the deformation of the upper crust [*Jahr et al.*, 2006]. In Figure 1 the site as well as the distribution of tiltmeters and the data transfer to KTB is shown.

3. Tiltmeter Experiment

[7] The tiltmeter array, consisting of five high-resolution ASKANIA borehole tiltmeters, was arranged around KTB in distances between 1.5 and 3.3 km to the injection borehole, the installations taking place at different geological settings [*Jahr et al.*, 2006; Figure 1]. The distance of the expected maximum tilt signal was estimated by numerical pre-modeling using an analytical approach as well as the finite-element-method (FEM [*Wang and Kümpel*, 2003; *Jahr et al.*, 2005]). This investigation also reveals, that a maximum tilt angle of about 6 msec (~30 nrad) could be expected about 4 months after the start of the injection, increasing. In addition, injection-induced seismicitiy was observed by a borehole geophone, installed in the KTB-HB and by a local seismic network, operated by GFZ-Potsdam, consisting of more than 30 seismic stations [*Shapiro et al.*, 2006].The deployed ASKANIA borehole tiltmeters with a nominal resolution better than 0.2 msec (~1 nrad) belong to

Plugs of the two ortho-
gonal components of
the tiltmeter

Cable of the
seismic signal

Light emitting diodes
(LED), used for the
optical estimation of
the tiltmeter orientation

horizontal and vertical
geophones (4.5Hz)

Head of the ASKANIA
borehole tiltmeter, built
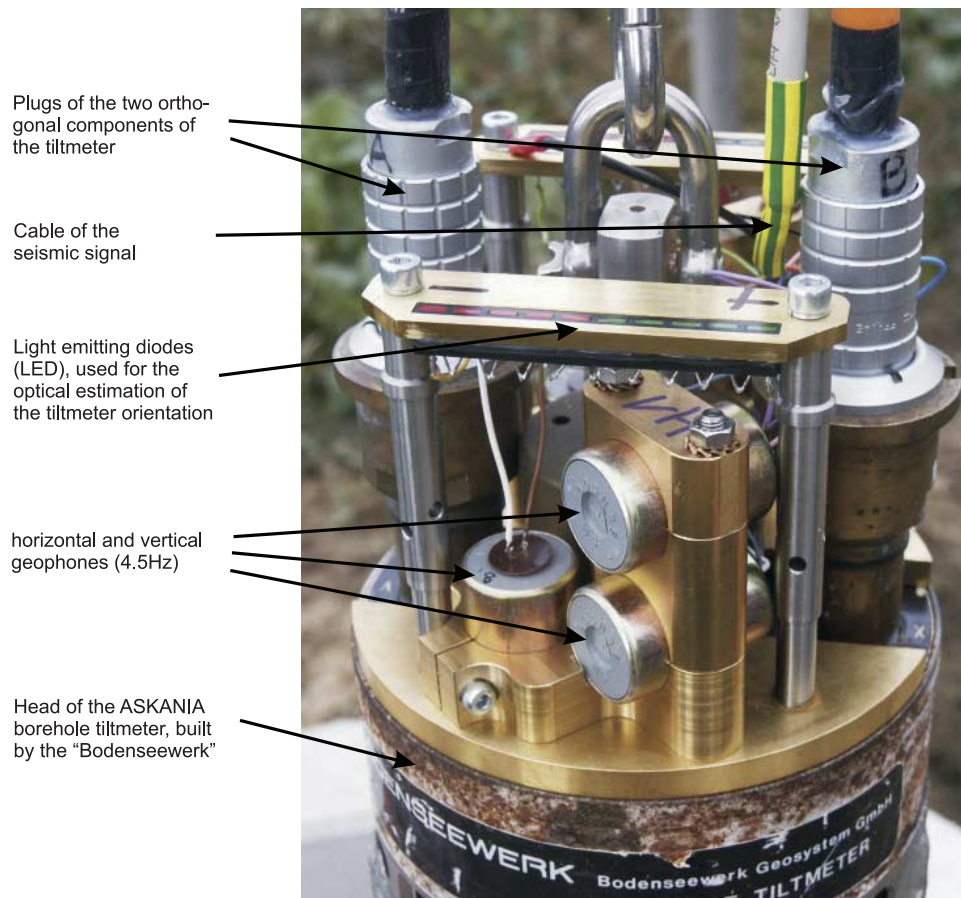by the "Bodenseewerk"

Figure 2. Modified head of the ASKANIA borehole tiltmeter: The diameter of the tiltmeter is 0.14 m, the total length of the tiltmeter tube 1.60 m. The effective tiltmeter length of 0.60 m yields an eigenfrequency of ∼0.7 Hz [*Gebauer et al.*, 2007].

the most sensitive tiltmeters worldwide [*Weise et al.*, 1999; *Gebauer et al.*, 2007]. Using this tiltmeter type the observed tilt due to tidal deformation of the Earth (∼20 msec) provides a dominant harmonic signal. However, the high instrumental sensitivity needs protection against environmental influences, like changes of meteorological parameters and groundwater level. Therefore, the tiltmeters need to be installed in boreholes at depths of at least 30 m, well coupled to the surrounding solid rocks.

[8] With such tiltmeters we already worked in different places following various goals: Earth tides and ocean/atmosphere loading in Finland [*Weise et al.*, 1999], reservoir loading in Norway [*Jentzsch and Koss*, 1997], as well as tectonic signals and ocean loading in the observatory Nokogiriyama in Japan [*Ishii et al.*, 2001]. Proper installations in boreholes up to 60 meters deep or in shallow boreholes in galleries allow to benefit from the resolution of these tiltmeters and their long-term stability. For the tiltmeter array at the KTB site the tiltmeters were additionally equipped with 3-component geophones (4.5 Hz) in order to complement the local seismic array for the monitoring of injection-induced seismicity (Figure 2).

[9] An unexpected observation occurred in connection with the large Sumatra-Andaman earthquake, 26 December 2004 [see, e.g., *Stein and Okal*, 2005]. For the first time the induced free modes of the Earth, especially the toroidal modes, could be observed with our array of tiltmeters. This allowed the stacking of the resulting spectra, with a corresponding high signal-to-noise ratio to enable the separation of different toroidal modes normally not observable [*Jentzsch et al.*, 2005]. This high-resolution observation can be used for the advancement of existing Earth models [cf., *Park et al.*, 2005].

4. Experimental Results

[10] The observed injection-induced tilt is separated after the reduction of linear instrumental drifts, barometric pressure and seasonal groundwater influences. Then, the movements of pendulum tips above ground show the induced deformation during the injection period (Figure 3). The stations Mittelberg and Eiglasdorf (cf., Figure 1) show tilts away from the injection point between October 2004 (yellow dots in Figure 3) and end of injection (red dots in Figure 3). Station Berg, which is the closest station to the injection point, shows tilt away from the injection point from the start of injection (green point in Figure 3) up to October 2004 and during the relaxation period (between red and black dots in Figure 3). The green arrows in Figure 3 indicate the modeled tilts for the homogeneous case. Further, east-west tilts are visible for Mittelberg and Berg and north-east to south-west tilt for Eiglasdorf, which indicate
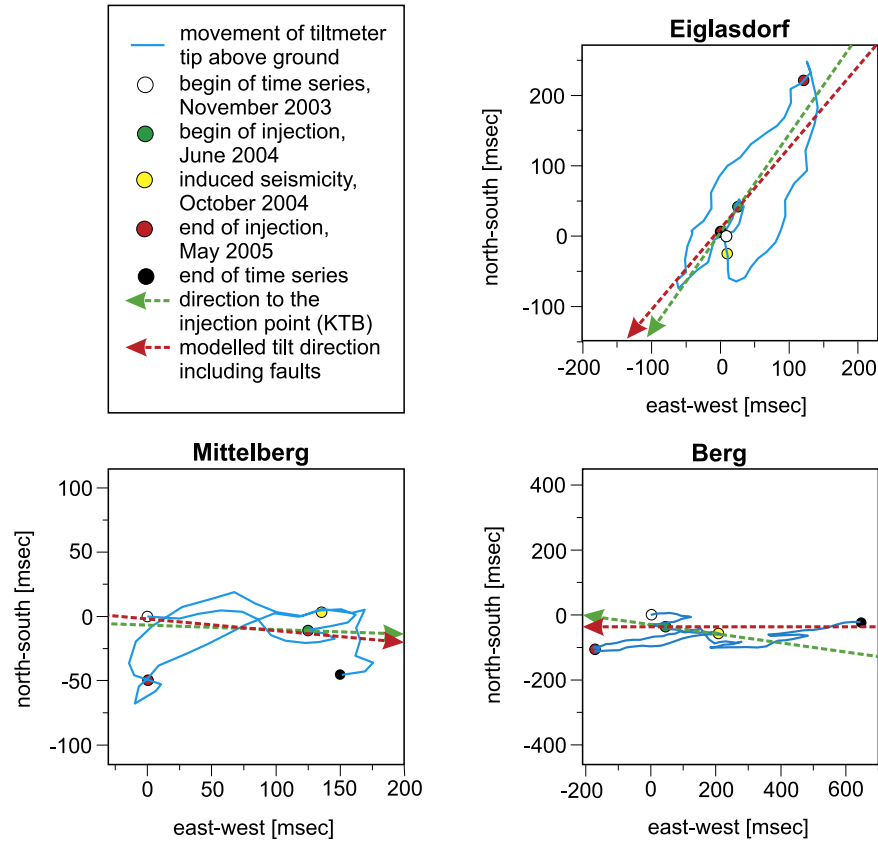
Figure 3. Observed movement of the tip of the pendulums above ground during injection. An upward movement of the trace indicates tilt to north, a trace movement to the left side indicates a tilt to west, and vice versa for south and east tilting. Mittelberg is located west; Berg, east; and Eiglasdorf, north-east of the injection borehole (cf., Figure 1, discussion see text). The green arrows indicate the general trends of the tilt at each station for the homogeneous case. The red ones show the modeled tilt direction, when fault zones are taken into account (cf., discussion in chapter 6).

that the relaxation process of the previous production test from June 2002 to June 2003 was not totally completed at the beginning of the tilt observations in November 2003. For the production test and the relaxation period it can be assumed, that the backflow water paths are the same, which are activated by the injection, therefore the main tilt orientations, east-west for Mittelberg and Berg and north-east to south-west for Eiglasdorf, look always similar. However, poro-elastic modeling only explains the observed induced bulge, not the observed time shifts between the tilts in Mittelberg and Eiglasdorf on the one side (October 2004 until May 2005) and Berg on the other side (June 2004 until autumn 2004).

[11] The station Stockau was twice destroyed by lightning, and in Püllersreuth strong groundwater influences are superimposed. At these two sites the deformation signal was masked by strong disturbances or data gaps, but the expected bulge due to the injection was clearly detected by three stations of the tiltmeter array.

5. Numerical Modeling

[12] The interpretation of the observed induced deformation was based on numerical investigation with the finite element method (FEM), using the software package ABAQUS [ABAQUS, 2006]. The 3-dimensional model, based on a poro-elastic rheology, includes the main geological settings and the main fault zones, like the seismic reflectors SE1, SE2, SE4 and the Nottersdorf Fault Zone (NdS).

[13] Following ABAQUS [2006] the volume change, which is observed as deformation at the surface, can be explained by pore pressure changes. During elastic processes in a porous elastic medium the pore volume e is in relation to the logarithmic surrounding stress p given by

$$p = -\frac{1}{3}(\sigma_{11} + \sigma_{22} + \sigma_{33}) \qquad (1)$$

and

$$\delta e^{el} = -\kappa\delta(\ln(p)). \qquad (2)$$

The material parameter κ is dimensionless and called *logarithmic bulk modulus* in ABAQUS [2006], and the index *el* denotes the elastic case. κ is given by the ratio of the pore-volume changes and the logarithmic stress-field of the surrounding area.
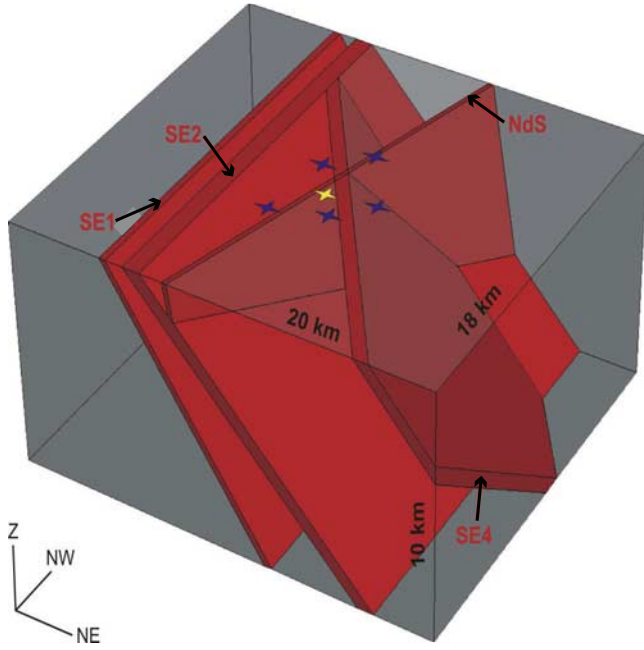
Figure 4. Finite-element model with dimensions, main fault zones SE1, SE2, NdS and SE4, which correspond to seismic reflectors, the KTB injection point (yellow star) and the tiltmeter array (blue stars): Note that the model is rotated 45° westward against north, in order to keep the model boundary parallel to the main faults SE1 and SE2. The rotation axis is equivalent to the center of the model at the injection borehole at KTB (yellow star). Widths of faults: SE1, 247 m; SE2, 588 m; NdS, 147 m; SE4, 444 m (depending on geological findings and element size). Geometrical and rheological parameters of this model are summarized in Table 1.

[14] Regarding the tensile strength of the material the possible tension up to the irreversible deformation has to be considered:

$$\delta e^{el} = -\kappa \delta\big(\ln\big(p + p_t^{el}\big)\big) \quad (3)$$

with p_t^{el} as elastic tensile strength of the material. If we neglect the compressibility of the solid and the fluid material, the elastic volume change J^{el} is defined as:

$$J^{el} = \frac{1 + e^{el}}{1 + e_0} \quad (4)$$

whereas e^{el} is the pore volume during a pure elastic deformation and e_0 the initial pore volume. The substitution yields:

$$\frac{\kappa}{1 + e_0} \ln\left(\frac{p + p_t^{el}}{p_0 + p_t^{el}}\right) = 1 - J^{el} \quad (5)$$

with p_0 as initial surrounding stress.

[15] Beside the normal acting main stresses the shear stress S has to be considered. This can be realized by assuming a constant shear modulus G as:

$$S = 2Ge^{el} \quad (6)$$

or if Poisson's ratio ν is known:

$$\delta S = 2G\delta e^{el} \quad (7)$$

with

$$G = \frac{3(1 - 2\nu)(1 + e_0)}{2(1 + \nu)\kappa}\big(p + p_t^{el}\big)\exp\big(\varepsilon_{vol}^{el}\big). \quad (8)$$

[16] The term ε_{vol}^{el} describes the elastic part of volume change. In addition to the elastic response of the pore volume the volume changes of the fluid and of the solid material are important. For the fluid of the model system we assumed:

$$\frac{\rho_w}{\rho_w^0} \approx 1 + \frac{u_w}{K_w} - \varepsilon_{vol}^{th} \quad (9)$$

whereas ρ_w is the actual density, ρ_w^0 the reference density, u_w the pore pressure and K_w the bulk modulus of the fluid. ε_w^{th} describes the volume change due to temperature variations; corresponding to (9) the solid material is given by:

$$\frac{\rho_g}{\rho_g^0} \approx 1 + \frac{1}{K_g}\left(su_w + \frac{\overline{p}}{1 - n}\right) - \varepsilon_g^{th} \quad (10)$$

The index g marks the properties of the solid, s is the saturation of the pores with fluid, n the porosity of the medium and $\overline{p}$ the mean surrounding stress inside the medium. Thus the term $-u_w/K_g + \varepsilon_g^{th}$ reflects the part of the volume change, which is caused by the acting pore pressure and thermal processes. This volume change causes a deformation also close to the surface of the model, which was detected as tilt changes in the real injection experiment at KTB.

[17] The boundary conditions are composed in that the total injection-induced pore pressure changes do not affect geological bodies which are more than 6 km away from the injection drill hole and not deeper than 6 km from the injection point. Therefore, the model dimension was chosen to 20 × 18 km in horizontal and 10 km in vertical direction. Further, we assume that the whole injection process can be described by a poro elastic model, temperature effects not included. The tiltmeter stations, the model dimensions and the striking and dipping of the fault zones are shown in Figure 4. The FE model consists of 25,600 elements of hexahedron type, with a mean element size of 525 m. However, the finite element mesh was generated with higher resolution inside the fault zones. For a poro elastic rheology the main fault zones are characterized by an increased permeability. All parameters characterizing the developed finite element model are compiled in Table 1, including elastic and poro elastic parameters for the faults, the surrounding rocks and the fluid. They were derived from the studies of *Endom and Kümpel* [1994], *Gräsle et al.*

Table 1. Model Parameters

Model Parameter	Quantity/Source	References
Model extension horizontal	20×18 km^2	*Lau* [2007]
Model extension vertical	10 km	*Lau* [2007]
Element type	Hexahedron	*Lau* [2007]
Number of elements	25,600	*Lau* [2007]
Number of faults	4	*Lau* [2007], *Dill et al.* [1991]
Geological structure and tectonics	Papers on potential field analyses and reflexion seismics	*Bosum et al.* [1997], *Brudy et al.* [1997], *Clauser et al.* [1997], *Harjes et al.* [1997]
Width of faults SE1, SE2	247 m, 588 m	*Lau* [2007], *Dill et al.* [1991]
Width of faults NdS, SE4	147 m, 444 m	*Lau* [2007], *Dill et al.* [1991]
Density	2832 kg/m^3	*KTB Data bank* [2006]
Hydraulic conductivity (rocks)	5×10^{-12} m/s	*Gräsle et al.* [2006]
Hydraulic conductivity (faults)	5×10^{-9} m/s	*Gräsle et al.* [2006]
Void ration	0.0101	*Huenges et al.* [1997]
Specific fluid weight	10,104.3 N/m^3	*McDermott et al.* [2006]
Logarithmic bulk modulus	0.005	*Lau* [2007], *ABAQUS* [2006]
Poisson ration	0.249	*Endom and Kümpel* [1994]
Bulk modulus rocks	7.937×10^{10} Pa	*Endom and Kümpel* [1994]
Bulk modulus fluid	2.22×10^9 Pa	*Endom and Kümpel* [1994]
Loading, step 1: gravity	9.81 m/s^2	*Lau* [2007]
Loading, step 2: regional stress in 2 km, 6 km, 9 km depth	28.8 MPa, 113.5 MPa, 183 MPa	*Baumgärtner et al.* [1990], *Brudy et al.* [1997]
Loading, step 3: injection pressure	11.46 MPa	*Gräsle et al.* [2006]

[2006], *Huenges et al.* [1997], *McDermott et al.* [2006] and from the *KTB Data bank* [2006].

6. Modeling Results and Interpretation

[18] The model was loaded by the Earth's gravity and the main horizontal stress field of Central Europe [*Zoback and Fuchs*, 1989; *Müller et al.*, 1992]. Then, this pre-loaded model was injected with the real injection rate and the periods of injection [*Kümpel et al.*, 2006]. The main fault zones are characterized by an increased permeability compared to the surrounding rock (Table 1). The resulting stress and deformation fields were investigated and compared with the observed deformation, derived from the tiltmeter array around KTB.

[19] The modeled tilt and its time evolution is shown in Figure 5. The homogeneous effect is subtracted, such that in Figure 5a, no tilt is to be seen, Figure 5b shows the tilt after 10 months injection, and Figure 5c shows the final situation after another 12 months of relaxation is given

(after 22 months in all). The effect of the fault structure on the stress distribution is shown in Figure 6: In the homogeneous case a more or less radial symmetric stress field is obvious (Figure 6, left), whereas the influence of the fault zones leads to a strongly asymmetric stress distribution (Figure 6, right).

[20] The modeled pore pressure and the pore pressure due to the injection along the SE2 fault is shown in Figure 7. The injection-induced deformation along SE2 and the deformation field around the cross-line of SE2 and NdS close to the injection point is shown by Figure 8. Corresponding to the expectation the hydrostatic pressure is dominating the total pore pressure and reaches about 100 MPa at the bottom of the model in 10 km depth (Figure 7). The pore pressure changes caused by the injection is covered by the total effect, however the subtraction of the gravity induced pressure shows the pore pressure distribution due to injection along the SE2 fault. Close to the injection point a maximum pore pressure of more than 11 MPa is calculated (Figure 7) and the crossing
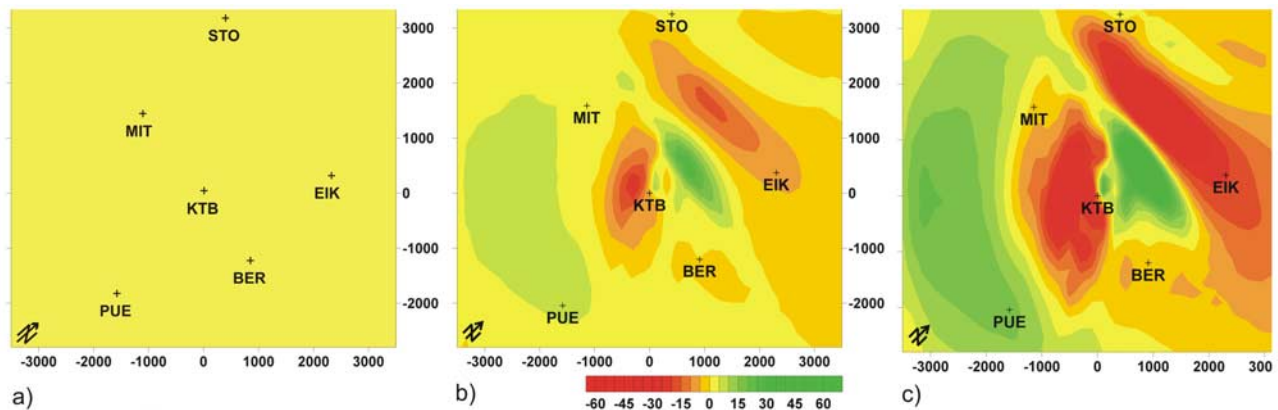

Figure 5. Modeled tilt, homogeneous effect removed: (a) start of injection; (b) 10 months later; (c) 22 months later (12 months after termination of injection).
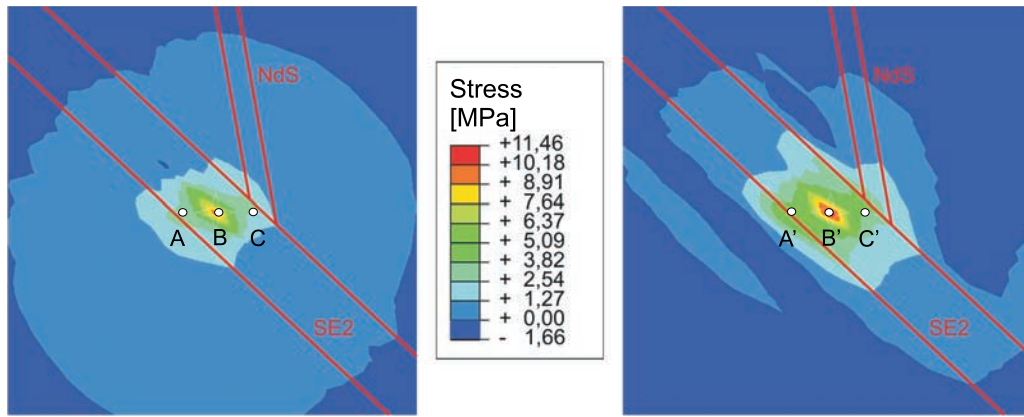
Figure 6. Comparison of stress accumulation: (left) Homogeneous case and (right) stress due to fault zones. Close to the injection point the stress magnitude increases by more than 20% (A′-A: 27%, B′-B: 23%, C′-C: 29%). Remark: The homogeneous case was achieved by setting the physical parameters of the fault zones to the values of the surrounding region. Thus the discretization of the fault zones causes small deviations from radial symmetry.

area to the NdS fault also affects the distribution of pore pressure around the injection point. The process of coupled deformation (Figure 8) is also clearly concentrated to this area. The connected propagation inside SE2 and NdS faults upward shows that the maximum deformation effect at the surface is in the order of some millimetres. The deformation map of the Earth's surface around the injection point shows maximum vertical uplift of over 3 mm caused by the injection, and tilts of more than 100 msec or ∼500 nrad (Figure 9).

[21] The investigation of pore pressure and deformation near the injection point yields the main results (Figures 7–9 and Table 2):

[22] 1. Fault zones affect the induced tilt orientation during the injection period, however, major deviations from the pure radial symmetry were modeled for the relaxation after end of injection. The injection-induced bulge and pore pressure stress were irregularly relieved by the backflow of the fluid inside the fault zones (Figure 5). Here, the influence of the fault zones (shown in Figure 4) becomes clearly visible: The red areas in Figure 5c correspond to the striking of the faults SE2 and SE4.

[23] 2. Fault zones increase the magnitude of stress accumulation and deformation by about 20% compared to a homogeneous block model. Induced fluids are concentrated in the high permeable fault zones, whereas in the case of homogeneity the fluids move radially in all directions (Figure 6). At the crossway of the faults at point C the stress change even amounts to nearly 30%.

[24] 3. The induced pore pressure variation is significantly controlled by the fault zones, especially by crossways of two faults like SE2 and NdS. However, SE4 northward dipping affects only station Eiglasdorf by about 40 msec, whereas influences of SE1 on the fluid distribution are not detectable. Including the faults in the modeling the computed tilts fit better to the observed ones. This is shown particularly for station Berg in Figure 3. These results reveal that the location, striking and dipping of the fault zones are most important for the fluid propagation and for the resulting stress accumulation (Figures 5, 7, 8, and 9).
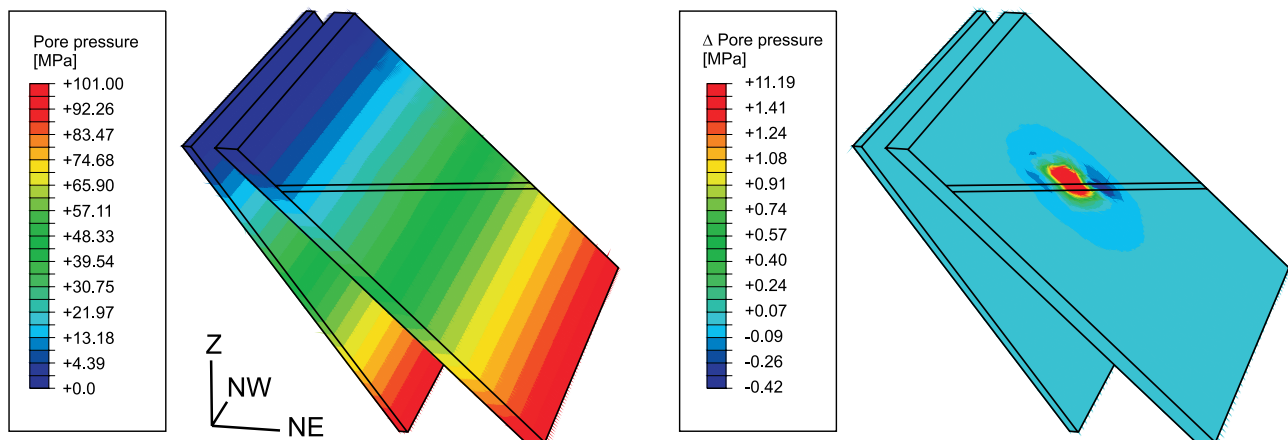

Figure 7. Modeled pore pressure distribution along the SE2 fault. (left) The total effect results in approximately 100 MPa at the bottom of the model, which is consistent with the hydrological pressure. (right) The subtraction of the gravity effect yields the pure injection-induced pore pressure.
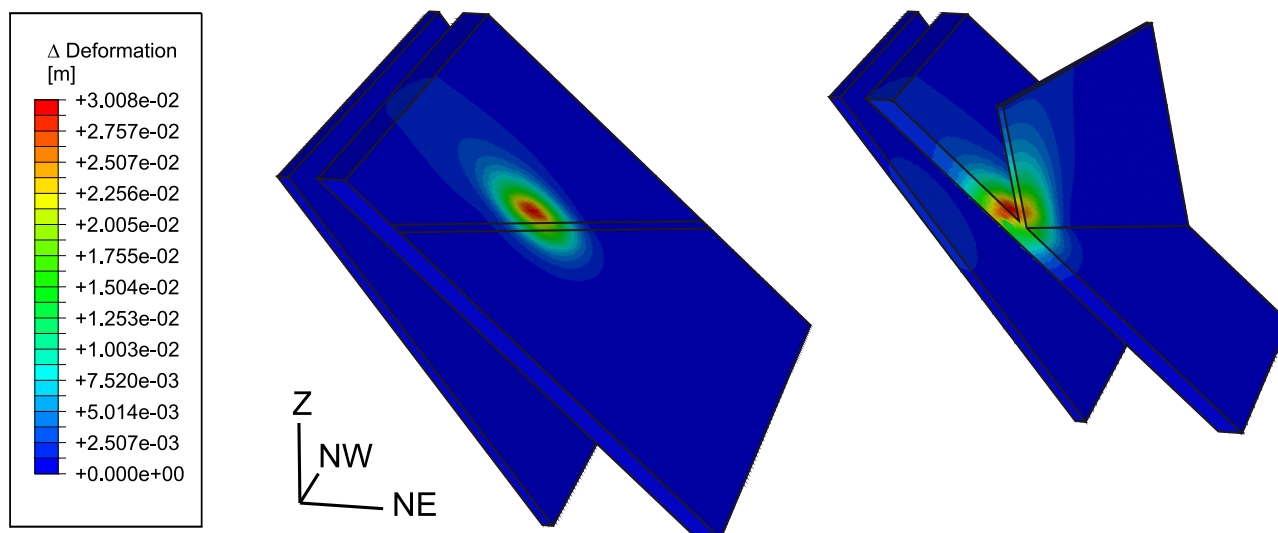
Figure 8. (left) Modeled injection-induced deformation along the SE2 fault and the induced deformation field at the crossing area of SE2 and NdS faults. (right) Only the half model close to the injection point is shown.

[25] 4. The region of maximum deformation is located north of the injection point, slightly striking in north-west to south-east direction. This correlates clearly with the observed induced seismicity, which occurred also in this region (Figure 9; cf., *Kümpel et al.* [2006], *Shapiro et al.* [2006]).

[26] 5. The whole induced geodynamic process including the relaxation process kept on several months after the end of injection. The fluid migration upward occurred along the faults NdS and SE2 (Figure 8). The correlated deformation variations were also observed by the tiltmeter array about 12 months after the end of the injection, and the poro-elastic modeling results confirm these observations (cf., experimental results in Figure 3).

[27] The obvious conformity of areas of maximum deformation and induced seismicity (point 4), i.e., the seismological results of *Shapiro et al.* [2006] and the modeling of *Lau* [2007] yield the following conclusion: The Mohr-Coulomb-criterion describes the required critical shear stress τ_{crit} for the crack with a normal stress σ_n on the potential fraction surface, including the cohesion c and the coefficient of friction μ [*Eisbacher*, 1991]:

$$\tau_{crit} = c + \mu\sigma_n. \tag{11}$$

For the area under investigation at the KTB *Shapiro et al.* [2006] show, that induced seismicity is triggered at the hypocenters already at very low pressure variations of less than 0.1 MPa. This signifies that the normal stress has to be close to the critical shear stress, and that the injection needs to reduce the frictional shear resistant only by small value. However, the observed induced seismicity occurred after 110 days after the start of injection. At this time the fluid volume, which was extracted during the pump test from 2002 to 2003, was refilled by the injection.

[28] In the frame of the poro-elastic modeling presented here, *Lau* [2007] showed, that the consideration of the regional stress field reveals an additional maximum tilt effect of only 2 msec and therefore the injection process yields a much higher contribution to the observed deformation.

[29] These results show that the whole geodynamic process is controlled by the migration paths of the injected fluid, dominated by the local fault zones, particularly the intersection of the faults SE2 and NdS close to the injection source. Consequently, the stress accumulation, the observed deformation and seismicity depend mainly on the structure and the fluid as controlling parameters of the concerned fault zones.

7. Conclusions

[30] This investigation shows in a large-scale experiment that fluid induced stress changes also cause deformation in the upper crust, and, thus, observable deformation of the surface. Small, but highly significant induced tilt signals were detected by the tiltmeter array around KTB after three months of injection with magnitudes between 100 msec and 150 msec. Modeling revealed that these tilt amplitudes correspond to a vertical uplift of 3.1 mm of the Earth's surface close to the injection borehole. The induced pore pressure changes of more than 11 MPa show highest values close to the injection point, but the induced deformation field has maximum values of ~3 cm north of the injection point in 4 km depth, close to the cross point of the faults SE2 and NdS. Both faults control the tilt orientation and magnitude, because they run close to the injection point and they are prone to efficient fluid transport due to high permeability. Therefore, at all stations different effects of the backflow are present superimposing the effect of injection. Thus the development of the bulge is not uniform but time-dependent. Our modeling presented here only describes the effect due to injection, not the combined effect of relaxation to pumping and injection. This extension of the numerical modeling is still pending.
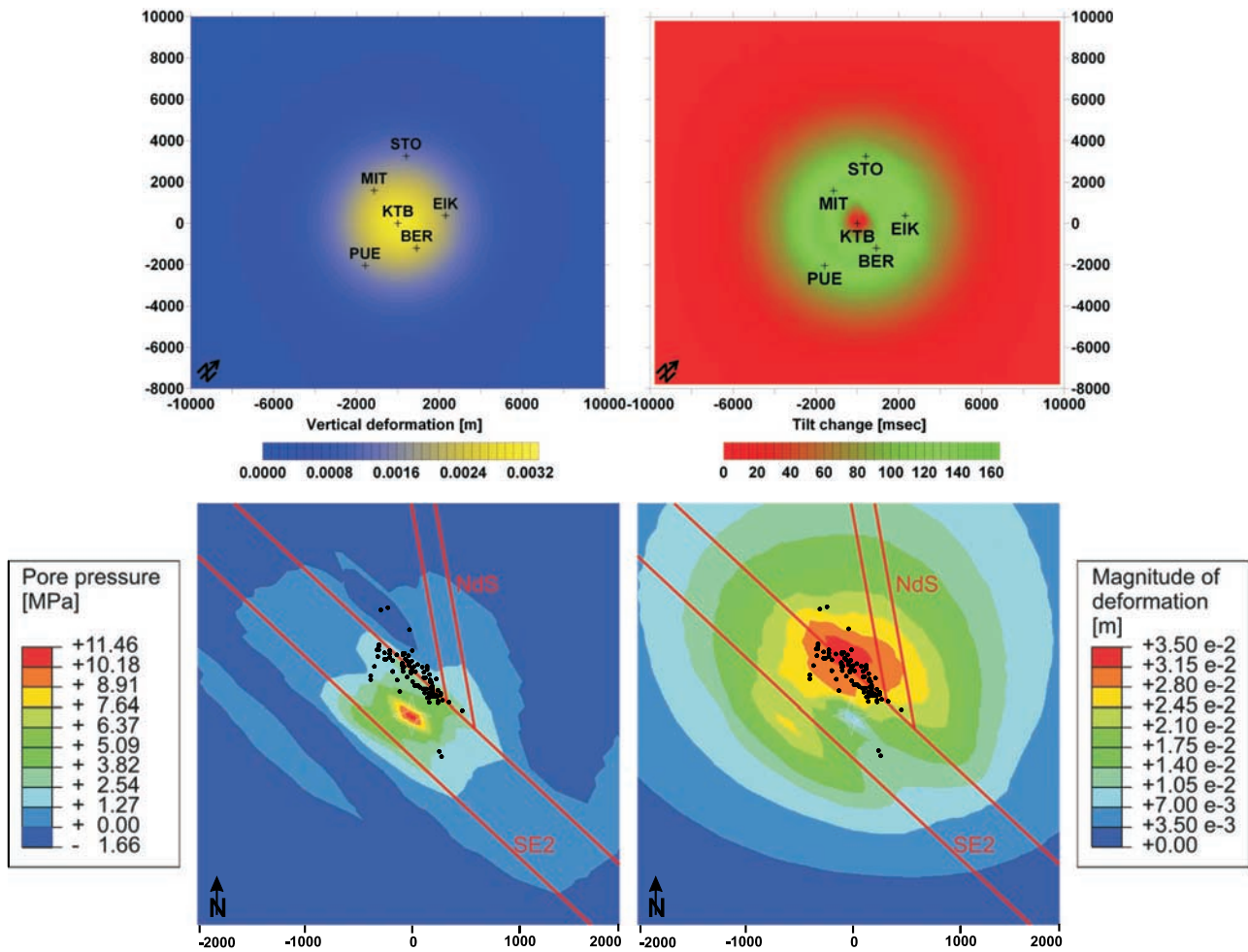
Figure 9. Results of the numerical interpretation of the injection experiment and observed seismicity. (a) Vertical deformation at the surface; (b) tilt changes at the surface; (c) pore pressure; and (d) deformation near the injection point in 4 km depth. Black dots mark the injection-induced seismic events. The area of induced seismicity is not correlated with the area of maximum pore pressure but with the area of maximum deformation, which is close to the crossway of the SE2 and the NdS faults in 4 km depth. Results of the modeling and the observed seismicity are summarized in Table 2.

[31] It can be concluded that the deformation field depends strongly on the geometry and the permeability of the concerned fault zones and local geological features. This demonstrates how fluids control the stress and deformation fields of the upper crust. It is shown that the observation of even very small injection-induced deformation enables a three dimensional high-resolution evaluation of the ongoing geodynamic process and the correlation to the observed induced seismicity. Thus tilt changes and induced seismicity as independent monitoring methods point to identical areas of stress accumulation in the upper crust.

[32] In a further step we hope to extend our model to explain the temporal evolution of the induced bulge. The results should also help to interpret tectonic processes, based on both, observation and numerical modeling, thus, the application of our findings to tectonically active areas, like swarm earthquake regions, high-risk areas near volcanoes or continental plate boundaries. In volcanic areas fluid/magma migration plays a major role [*Battaglia et al.*, 1999], whereas at plate boundaries tectonic stress is the main driving force [*Nadeau and McEvilly*, 2004]. All this can only be done on the basis of high-resolution tiltmeters which were fortunately available for the observation period, provided by our Geodynamic Observatory Moxa [*Jahr et al.*, 2001].

Table 2. Modeling and Seismological Results

Modeling Result	Quantity
Maximum pressure increase	11.5 MPa
Maximum fluid flow velocity	5×10^{-10} m/s
Maximum deformation (in source region)	0.0350 m
Maximum vertical deformation (at surface)	0.0032 m
Maximum surface tilt	~150 ms
Seismological Result	
Number of events detected by KTB-HB borehole geophone	About 3000
Number of events detected by local seismic network at the surface	150
Depth of earthquake foci	3500–4500 m

References

ABAQUS, Inc. (2006), ABAQUS Documentation, Version 6.1.1, ABAQUS, Inc., R. I.

Baisch, S., and H.-P. Harjes (2003), A model for fluid-injection-induced seismicity at the KTB, Germany, *Geophys. J. Int.*, 152, 160–170.

Battaglia, M., C. Roberts, and P. Segall (1999), Magma intrusion beneath Long Valley Caldera confirmed by temporal changes in gravity, *Science*, 285(5436), 2119–2122.

Baumgärtner, J., F. Rummel, and M. Zoback (1990), Hydraulic fracturing in situ stress measurements to 3 km depth in the KTB pilot hole VB, *KTB Rep.*, vol. 90–6a, pp. 353–399.

Bosum, W., U. Casten, F. Fieberg, I. Heyde, and H. Soffel (1997), Three-dimensional interpretation of the KTB gravity and magnetic anomalies, *J. Geophys. Res.*, 102(B8), 18,307–18,321.

Bräuer, K., H. Kämpf, S. Niedermann, and G. Strauch (2005), Evidence for ascending upper mantle-derived melt beneath the Cheb basin, central Europe, *Geophys. Res. Lett.*, 32, L08303, doi:10.1029/2004GL022205.

Brudy, M., M. Zoback, K. Fuchs, F. Rummel, and J. Baumgärtner (1997), Estimation of the complete stress tensor to 8 km depth in the KTB scientific drill holes: Implications for crustal strength, *J. Geophys. Res.*, 102(B8), 18,453–18,475.

Clauser, C., P. Giese, E. Huenges, T. Kohl, L. Lehmann, H. Rybach, J. Savanda, H. Wilhelm, K. Windloff, and G. Zoth (1997), The thermal regime of the crystalline continental crust: Implications from the KTB, *J. Geophys. Res.*, 102(B8), 18,417–18,441.

Dill, H., B. Schröder, G. Stettner, and G. Hirschmann (1991), *Geologische Karte des KTB-Umfeldes Oberpfalz 1:50.000*, Niedersächsisches Landesamt für Bodenforschung und Bayerisches Geologisches Landesamt, Hannover.

Eisbacher, G. H. (1991), *Einführung in die Tektonik*, Ferd. Enke Verlag, Stuttgart.

Emmermann, R., and J. Lauterjung (1997), The German Continental Deep Drilling Program KTB: Overview and major results, *J. Geophys. Res.*, 102(B8), 18,179–18,202.

Endom, J., and H. J. Kümpel (1994), Analysis of natural well level fluctuations in the KTB-Vorbohrung: Parameters from poroelastic aquifer and single fracture models, *Sci. Drill.*, 4, 147.

Fujimori, K., H. Ishii, A. Mukai, S. Nakao, S. Matsumoto, and Y. Hirata (2001), Strain and tilt changes measured during a water injection experiment at the Nojima Fault zone, *Jpn. Isl. Arc*, 10, 228.

Gebauer, A., T. Jahr, and G. Jentzsch (2007), Recording and interpretation/analysis of tilt signals with five ASKANIA borehole tiltmeters at the KTB, *Rev. Sci. Instrum.*, 78/5, 6.

Gräsle, W., W. Kessels, H. J. Kümpel, and X. Li (2006), Hydraulic observations from a one year fluid production test in the 4000 m deep KTB pilot borehole, *Geofluids*, 6, 8.

Haak, V., and A. G. Jones (1997), Introduction to special section: The KTB deep drill hole, *J. Geophys. Res.*, 102(B8), 18,175–18,177.

Harjes, H.-P., et al. (1997), Origin and nature of crustal reflections: Results from the integrated seismic measurements at the KTB superdeep drilling site, *J. Geophys. Res.*, 102(B8), 18,267–18,288.

Harms, U., C. Koeberl, and M. D. Zoback (2007), *Continental Scientific Drilling*, Springer, Berlin.

Hill, D. P., and S. Prejean (2005), Magmatic unrest beneath Mammoth Mountain, California, *J. Volcanol. Geotherm. Res.*, 146, 257.

Huenges, E., J. Erzinger, J. Kück, B. Engeser, and W. Kessels (1997), The permeable crust: Geohydraulic properties down to 9101 m depth, *J. Geophys. Res.*, 102(B8), 18,255–18,265.

Ishii, H., G. Jentzsch, S. Graupner, S. Nakao, M. Ramatschi, and A. Weise (2001), Observatory Nokogiriyama/Japan: Comparison of different tiltmeters, *J. Geod. Soc. Jpn.*, 47/1, 155–160.

Jahr, T., G. Jentzsch, and C. Kroner (2001), The Geodynamic Observatory Moxa/Germany: Instrumentation and purposes, *J. Geod. Soc. Jpn.*, 47, 34–39.

Jahr, T., G. Jentzsch, H. Letz, and M. Sauter (2005), Fluid injection and surface deformation at the KTB location: Modelling of expected tilt effects, *Geofluids*, 5, 20–27.

Jahr, T., H. Letz, and G. Jentzsch (2006), Monitoring fluid induced deformation of the earth's crust: A large scale experiment at the KTB location/German, *J. Geodyn.*, 41(1–3), 190–197.

Jentzsch, G., and S. Koss (1997), Interpretation of long-period tilt records at Blå Sjø, Southern Norway, with respect to the variations of the lake level, *Phys. Chem. Earth*, 22, 25–31.

Jentzsch, G., T. Jahr, H. Letz, and A. Gebauer (2005), Erdeigenschwingungen nach dem Sumatra-Erdbeben vom 26. Dezember 2004—beobachtet mit 5 ASKANIA-Bohrloch-Neigungsmesser an der KTB, *Mitt.-Dtsch. Geophys. Ges.*, 1/2005, 12–13.

KTB Data bank (2006), KTB - Kontinentales Tiefbohrprogramm Der Bundesrepublik Deutschland (KTB-Continental Deep Drilling Project). (Available at http://Www.Icdp-Online.De/Sites/Ktb/Welcome.Htm)

Kümpel, H. J., J. Erzinger, and S. Shapiro (2006), Two massive hydraulic tests completed in deep KTB borehole, *Sci. Drill.*, 3, 40–42.

Lau, T. (2007), Modellierung der Fluidinjektion in der Vorbohrung der KTB mittels der Finite-Elemente-Methode, p. 111, Dipl.-Thesis, Friedrich-Schiller-Univ., Jena, Germany.

Lippmann, J., J. Erzinger, M. Zimmer, S. Schloemer, L. Eichinger, and E. Faber (2005), On the geochemistrry of gases and noble gas isotopes (including ^{222}Rn) in deep crustal fluids: The 400 m KTB-pilot hole fluid production test 2002–03, *Geofluids*, 5, 52–66.

McDermott, C., M. Lodemann, I. Ghergut, H. Tenzer, M. Sauter, and O. Kolditz (2006), Investigation of coupled hydraulic-geomechanical processes at the KTB site: Pressure-dependent characteristics of a long-term pump test and elastic interpretation using a geomechanical facies model, *Geofluids*, 6, 67–81.

Miller, S. A., C. Collettini, L. Chiaraluce, M. Cocco, M. Barchi, and B. J. P. Kaus (2004), Aftershocks driven by a highpressure CO_2 source at depth, *Nature*, 427, 724–727.

Möller, P., H. Woith, P. Dulski, V. Lüders, J. Erzinger, H. Kämpf, A. Pekdeger, B. Hansen, M. Lodemann, and D. Banks (2005), Main and trace elements in KTB-VB fluid: Composition and hints to ist origin, *Geofluids*, 5, 28–41.

Müller, B., M. L. Zoback, K. Fuchs, L. Mastin, S. Gregersen, N. Pavoni, O. Stephansson, and C. Ljunggren (1992), Regional patterns of tectonic stress in Europe, *J. Geophys. Res.*, 97(B8), 11,783–11,803.

Nadeau, M., and T. V. McEvilly (2004), Periodic pulsing of characteristic microearthquakes on the San Andreas Fault, *Science*, 303(5655), 220–222.

Park, J., et al. (2005), Earth's free oscillations excited by the 26 December 2004 Sumatra-Andaman earthquake, *Science*, 308, 1139–1144.

Raleigh, C. B., J. H. Healy, and J. D. Bredehoeft (1976), An experiment in earthquake control at Rangely, Colorado, *Science*, 191(4,233), 1230–1237.

Reches, Z., and H. Ito (2007), Scientific drilling in active faults, in *Continental Scientific Drilling*, edited by U. Harms, C. Koeberl, and M. D. Zoback, pp. 235–258, Springer, Berlin.

Shapiro, S. A., J. Kummerow, C. Dinske, G. Asch, E. Rothert, J. Erzinger, H. J. Kümpel, and R. Kind (2006), Fluid induced seismicity guided by a continental fault: Injection experiment of 2004/2005 at the German deep drilling site (KTB), *Geophys. Res. Lett.*, 33, L01309, doi:10.1029/2005GL024659.

Stein, R. S., and E. A. Okal (2005), Seismology: Speed and size of the Sumatra earthquake, *Nature*, 434, 581–582.

Stober, I., and K. Bucher (2005), The upper continental crust, an aquifer and its fluid: Hydraulic and chemical data from 4 km depth in fractured crystalline basement rocks at the KTB test site, *Geofluids*, 5, 8–19.

Tofani, G., and F. Horath (1990), Continuous tiltmeter monitoring to identify ground deformation mechanisms, *Geotechnical News*, June.

Wang, R., and H. J. Kümpel (2003), Poroelasticity: Efficient modeling of strongly coupled, slow deformation processes in a multilayered halfspace, *Geophysics*, 68, 705.

Weise, A., G. Jentzsch, A. Kiviniemi, and J. Kääriäinen (1999), Comparison of longperiod tilt measurements: Results from two clinometric stations Metsähovi and Lohja, Finland, *J. Geodyn.*, 27, 237–257.

Zoback, M., and K. Fuchs (1989), Probing the deep Crustal Stress Field and Brittle-Ductile Transition, *KTB Report 89-3*, A323–A324, 323.

Zoback, M. D., and H.-P. Harjes (1997), Injection-induced earthquakes and crustal stress at 9 km depth at the KTB deep drilling site, Germany, *J. Geophys. Res.*, 102(B8), 18,477–18,491.

————————
A. Gebauer, T. Jahr, and G. Jentzsch, Applied Geophysics, Institute of Geosciences, Friedrich-Schiller-University Jena, Burgweg 11, D-7749 Jena, Germany. (thomas.jahr@uni-jena.de)

T. Lau, Max-Planck-Institute of Meteorology, Bundesstrasse 53, 20146 Hamburg, Germany.